EBioMedicine 27 (2018) 138–150

Contents lists available at ScienceDirect

EBioMedicine

journal homepage: www.ebiomedicine.com

Research Paper

Mice with an Oncogenic HRAS Mutation are Resistant to High-Fat Diet-Induced Obesity and Exhibit Impaired Hepatic Energy Homeostasis

Daiju Oba [a], Shin-ichi Inoue [a,**], Sachiko Miyagawa-Tomita [b,c,d], Yasumi Nakashima [e], Tetsuya Niihori [a], Seiji Yamaguchi [f], Yoichi Matsubara [a,g], Yoko Aoki [a,*,1]

[a] Department of Medical Genetics, Tohoku University School of Medicine, Sendai, Japan
[b] Department of Pediatric Cardiology, Tokyo Women's Medical University, Tokyo, Japan
[c] Division of Cardiovascular Development and Differentiation, Medical Research Institute, Tokyo Women's Medical University, Tokyo, Japan
[d] Department of Veterinary Technology, Yamazaki gakuen University, Tokyo, Japan
[e] Department of Pediatrics, Seirei Hamamatsu General Hospital, Shizuoka, Japan
[f] Department of Pediatrics, Shimane University, Faculty of Medicine, Shimane, Japan
[g] National Research Institute for Child Health and Development, Tokyo, Japan

ARTICLE INFO

Article history:
Received 21 August 2017
Received in revised form 30 October 2017
Accepted 9 November 2017
Available online 6 December 2017

Keywords:
Costello syndrome
Hras G12S
Mitochondrial fatty acid oxidation
Diet-induced obesity
Cancer metabolism
ERK

ABSTRACT

Costello syndrome is a "RASopathy" that is characterized by growth retardation, dysmorphic facial appearance, hypertrophic cardiomyopathy and tumor predisposition. >80% of patients with Costello syndrome harbor a heterozygous germline G12S mutation in *HRAS*. Altered metabolic regulation has been suspected because patients with Costello syndrome exhibit hypoketotic hypoglycemia and increased resting energy expenditure, and their growth is severely retarded. To examine the mechanisms of energy reprogramming by *HRAS* activation *in vivo*, we generated knock-in mice expressing a heterozygous *Hras* G12S mutation ($Hras^{G12S/+}$ mice) as a mouse model of Costello syndrome. On a high-fat diet, $Hras^{G12S/+}$ mice developed a lean phenotype with microvesicular hepatic steatosis, resulting in early death compared with wild-type mice. Under starvation conditions, hypoketosis and elevated blood levels of long-chain fatty acylcarnitines were observed, suggesting impaired mitochondrial fatty acid oxidation. Our findings suggest that the oncogenic *Hras* mutation modulates energy homeostasis *in vivo*.

1. Introduction

Costello syndrome is a rare disorder with multiple congenital anomalies that is characterized by intellectual disability, high birth weight, postnatal growth retardation with feeding difficulties, curly hair, relative macrocephaly, dysmorphic facial features, loose skin, hypertrophic cardiomyopathy and a predisposition to malignancies (Costello, 1977; Hennekam, 2003). In 2005, we discovered that germline mutations in Harvey rat sarcoma viral oncogene homolog (*HRAS*) cause Costello syndrome (Aoki et al., 2005). Approximately 80% of patients with Costello syndrome have germline mutations in *HRAS*, which is one of the components of the RAS-MAPK signaling pathway (Aoki et al., 2005; Gripp et al., 2006; Kerr et al., 2006). Disorders resulting from germline mutations in components of the RAS-MAPK signaling pathway are now collectively referred to as RASopathies or RAS-MAPK syndromes, including Noonan syndrome, Costello syndrome, cardio-facio-cutaneous (CFC) syndrome, Noonan syndrome with multiple lentigines (LEOPARD syndrome) and neurofibromatosis type 1 (Aoki et al., 2016; Aoki et al., 2008; Rauen, 2013; Tidyman and Rauen, 2009).

Somatic *HRAS* mutations at residues 12, 13 and 61 are frequently found in bladder cancer, head and neck cancer, vulvar and cutaneous squamous cell carcinoma and lung cancer (Lawrence et al., 2014; McDaniel et al., 2014; Oliva et al., 2004; Trietsch et al., 2014; COSMIC database http://cancer.sanger.ac.uk/cosmic/gene/analysis?ln=HRAS). The most common somatic mutation at codon 12 of *HRAS* is the G12V mutation, c.35G > T (p.Gly12Val). In contrast, the most frequent germline mutation in Costello syndrome patients (>80%) is the *HRAS* G12S mutation, c.34G > A (p.Gly12Ser) (Aoki et al., 2005; Gripp et al., 2006; Kerr et al., 2006). It has been reported that the levels of the GTP-bound active form of *HRAS* G12V are higher than those of *HRAS* G12S (Wey et al., 2013). Two groups have developed Costello syndrome mouse models that express *Hras* G12V ($Hras^{G12V}$ knock-in mice). However, mice with the *Hras* G12S mutation, which is the most common mutation in Costello syndrome, have not been generated.

* Correspondence to: Y. Aoki, Department of Medical Genetics, Tohoku University School of Medicine, 1-1 Seiryo-machi, Aoba-ku, Sendai 980-8574, Japan.
** Correspondence to: S. Inoue, Department of Medical Genetics, Tohoku University School of Medicine, 1-1 Seiryo-machi, Aoba-ku, Sendai 980-8574, Japan.
E-mail addresses: sinoue@med.tohoku.ac.jp (S. Inoue), aokiy@med.tohoku.ac.jp (Y. Aoki).
[1] Lead Contact.

https://doi.org/10.1016/j.ebiom.2017.11.029

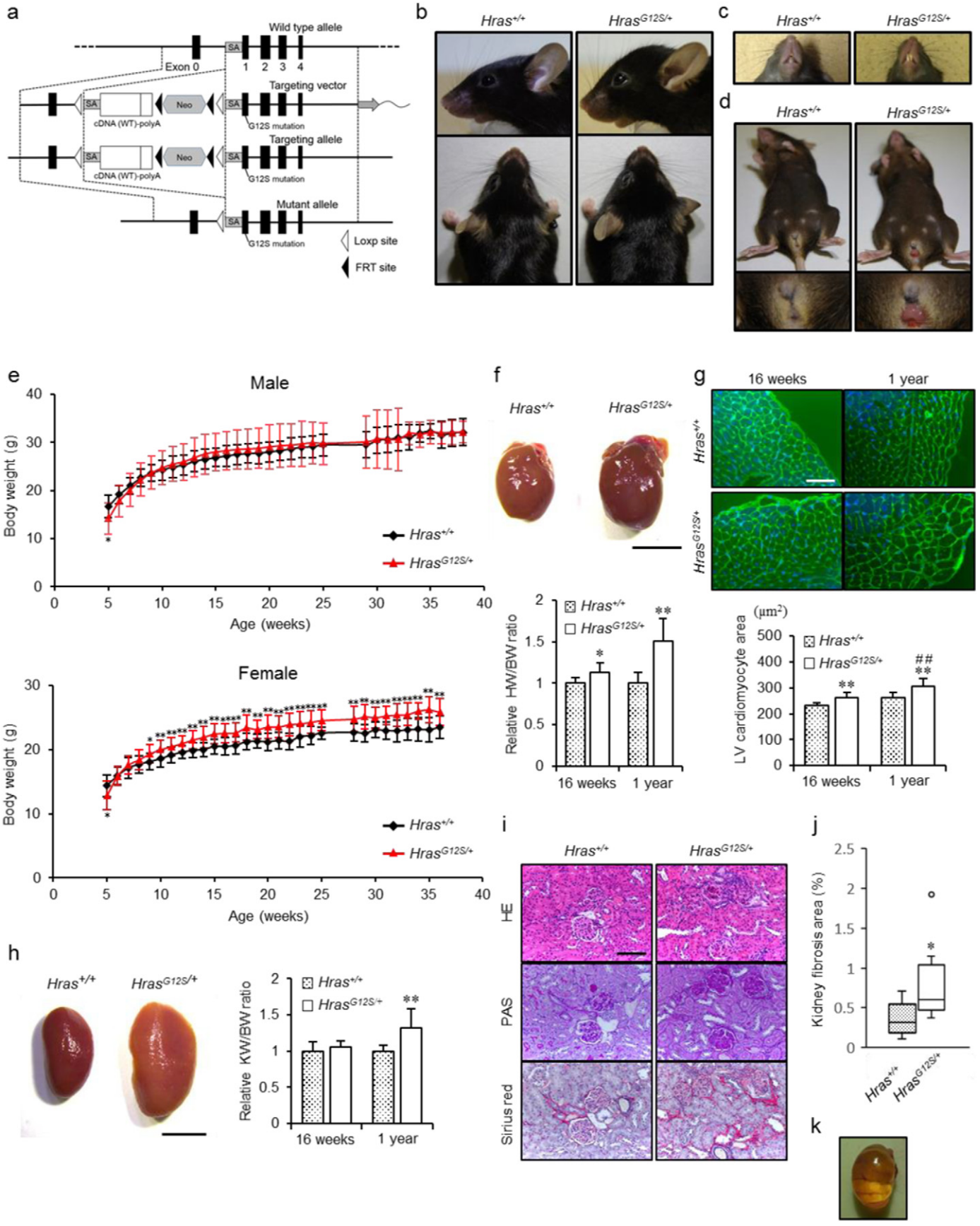
a
Wild type allele
Exon 0
SA
1 2 3 4
Targeting vector
Neo
cDNA (WT)-polyA
G12S mutation
Targeting allele
Mutant allele
Loxp site
FRT site
b
Hras+/+
HrasG12S/+
c
d
e
Male
Body weight (g)
Age (weeks)
Female
f
Relative HW/BW ratio
16 weeks
1 year
g
16 weeks
1 year
LV cardiomyocyte area (μm2)
h
Relative KW/BW ratio
i
HE
PAS
Sirius red
j
Kidney fibrosis area (%)
k

Costello syndrome patients with germline *HRAS* mutations exhibit fasting hypoglycemia with growth hormone and cortisol deficiencies, and hypoglycemia with or without decreased ketone bodies (Hennekam, 2003). Moreover, patients with Costello syndrome have resting energy expenditure, which indicates enhanced basal metabolism (Leoni et al., 2016). Recent studies have provided evidence that patients with RASopathies and associated mouse models exhibit mitochondrial dysfunction, including morphological defects, oxidative phosphorylation disorders and enzyme deficiencies in the oxidative phosphorylation system (Aeby et al., 2007; Kleefstra et al., 2011; Moriya et al., 2015). However, the metabolic homeostasis of individuals with oncogenic germline mutations (RASopathies) remains unclear. Recent studies have shown that cancer cells with RAS mutations exhibit altered metabolism characterized by enhanced glucose uptake, glycolysis, lipid synthesis and glutamine catabolism (Bryant et al., 2014; Zheng et al., 2015; Zhou et al., 2016). To gain an understanding of the effects of RAS activation on energy homeostasis *in vivo*, we generated knock-in mice expressing the Costello syndrome-associated *Hras* G12S mutation and examined energy homoeostasis in the liver.

2. Material and Methods

2.1. Generation of $Hras^{G12S}$ Knock-in Mice

Two BAC clones containing the *Hras* gene, ID: RP23-210J2 and RP-23-112C12, were used to generate the targeting vector. To construct the targeting vector for $Hras^{G12S}$ knock-in mice, DNA fragments including *Hras* exon 0, loxp-SA-Exon 1, *Hras* cDNA (Exon1–4)-polyA and SA-Exon1–4 were amplified using mouse BAC clones. These DNA fragments were ligated into the pBSIISK + or pBS vector. The *Hras* G12S (exon 1) mutation was introduced using site-directed mutagenesis. For construct 1, the loxp-SA-Exon 1 regions were inserted into the pBS vector containing *Hras* cDNA (Exon1–4)-poly A. For construct 2, the FRT-Neo-FRT-loxp cassettes and construct 1 fragments were inserted into the pBSIISK + vector containing *Hras* exon 0 DNA fragments. For the targeting vector, the construct 2 fragments were inserted into the pBSIISK + vector containing SA-Exon1–4 regions. The targeting vector was linearized with *Sal*I and electroporated into the C57B6-derived BRUCE-4 ES cells. We used genotyping and sequencing and tested the Cre-mediated recombination system to confirm the correctly targeted ES clones. Furthermore, homologous recombination was confirmed by Southern blotting using 5′, 3′ and Neo probes. The probe sequences are shown in Supplementary Table 1. Screened ES clones were then microinjected into BALB/c blastocysts, and the resulting chimeras were crossed with C57BL/6J mice to obtain $Hras^{G12S\ Neo/+}$ heterozygous mice. Excisions of the SA-*Hras* cDNA-poly A and Neo cassette were achieved by crossing the $Hras^{G12S\ Neo/+}$ heterozygotes with CAGCre transgenic mice on the C57BL/6J background (RIKEN BioResource Center, Tsukuba, Japan; RBRC01828) (Matsumura et al., 2004). To generate the $Hras^{G12S/+}$ mice, the $Hras^{G12S/+}$;*Cre* mice were crossed with C57BL/6 J mice (Charles River Laboratories Japan, Yokohama, Japan). All animal experiments were approved by the Animal Care and Use Committee of Tohoku University.

2.2. Genotyping

Genomic DNA was purified from mouse tail tissue using the Maxwell 16 Mouse Tail DNA Purification Kit (Promega, Madison, WI). Genotyping of $Hras^{+/+}$ and $Hras^{G12S/+}$ alleles was carried out by PCR amplification using KOD Fx Neo (TOYOBO, Osaka, Japan). The primers used for PCR were 5'-CGCTCAGTAAATAGTTGTAGGTTGC-3′ and 3′-CTCAGACCAGAGAATCCACAGAAC-5′.

2.3. Mouse Feeding and Care

The female mice were housed in a temperature-controlled room with a 12-h light/dark cycle and fed a conventional laboratory diet (control diet (CD); Labo MR Stock, Nosan Corporation Life-Tech Department, Yokohama, Japan) before weaning at 5 weeks of age. After weaning, the mice were fed a HFD containing 60% fat (HFD-60; Oriental Yeast Corporation, Tokyo, Japan) and housed in individual cages. The compositions of the Labo MR Stock and HFD-60 are shown in Supplementary Tables 2 and 3. Body weight and food intake were measured every 7 days.

2.4. Analysis of Serum Parameters

Mice were fed a HFD from 5 to 16 weeks of age. Serum samples from 16-week-old mice were obtained from the inferior vena cava while the mice were under anesthesia. The fasted blood samples were obtained after 24 h of fasting. All parameters were measured at the Oriental Yeast Corporation Nagahama Laboratory, Nagahama, Japan.

2.5. Measurement of Lipid Content

Liver and fecal samples were obtained from mice fed a HFD from 5 to 16 weeks of age. Total lipid extraction was performed by the Folch extraction procedure (Folch et al., 1957). The content of triglyceride, total cholesterol and free fatty acid were measured by using Triglyceride E-test Wako, Cholesterol E-test Wako and NEFA C-test Wako (Wako Pure Chemical Industries, Osaka, Japan), respectively.

2.6. Glucose and β-Hydroxybutyric Acid Measurement

Mice were fed a HFD from 5 to 16 weeks of age before the fasting test. Blood glucose and β-hydroxybutyric acid levels were measured after 0, 24 and 48 h of fasting. Samples were obtained from the tail veins of anesthetized mice and analyzed using a FreeStyle Precision Neo (Abbott Laboratories, Chicago, IL).

Fig. 1. Generation of *Hras* G12S knock-in mice and the $Hras^{+/+}$ and $Hras^{G12S/+}$ mouse phenotypes. (a) Gene-targeting strategy to generate the $Hras^{G12S/+}$ knock-in mice. Exons (solid boxes), neomycin cassettes (hexagonal boxes), *Hras* cDNA (Exons 1–4)-poly A cassettes (open boxes), splice acceptor sites (SA, labeled gray boxes), loxP sites (open arrowheads) and Flp recombination target (FRT) sites (solid arrowheads) are indicated. The SA-*HRAS* cDNA-poly A and Neo cassettes were removed by crossing with CAG-Cre transgenic mice. (b, c, d) Representative facial appearance, tooth arrangement and anal images of $Hras^{+/+}$ and $Hras^{G12S/+}$ mice. (b) The panels indicate the round facial appearance (upper panel) and shortened nasal bridge (lower panel) in $Hras^{G12S/+}$ mice compared with $Hras^{+/+}$ mice. (c) Malocclusion in $Hras^{G12S/+}$ mice. (d) Rectal prolapse in $Hras^{G12S/+}$ mice. (e) Body weights of male (upper graph) and female (lower graph) $Hras^{+/+}$ and $Hras^{G12S/+}$ mice fed a control diet (CD). The data are presented as the mean ± SD ($Hras^{+/+}$ (n = 17) and $Hras^{G12S/+}$ (n = 16) for males; $Hras^{+/+}$ (n = 17) and $Hras^{G12S/+}$ (n = 18) for females). $^{*}p < 0.05$, $^{**}p < 0.01$ (Welch's *t*-test) compared with $Hras^{+/+}$ mice. (f) Gross morphology of hearts from $Hras^{+/+}$ and $Hras^{G12S/+}$ mice at 1 year of age. The lower bar graph shows the heart weight (HW) to body weight (BW) ratios of $Hras^{+/+}$ and $Hras^{G12S/+}$ mice at 16 weeks and 1 year of age. The data are expressed as the mean ± SD ($Hras^{+/+}$ (n = 8) and $Hras^{G12S/+}$ (n = 8) at 16 weeks of age; $Hras^{+/+}$ (n = 10) and $Hras^{G12S/+}$ (n = 7) at 1 year of age). $^{*}p < 0.05$, $^{**}p < 0.01$ (Welch's *t*-test) compared with $Hras^{+/+}$ mice. Scale bar = 5 mm. (g) Transverse sections of wheat germ agglutinin-stained hearts from $Hras^{+/+}$ and $Hras^{G12S/+}$ mice at 16 weeks and 1 year of age. The lower bar graph shows the average area of left ventricular (LV) cardiomyocytes in $Hras^{+/+}$ and $Hras^{G12S/+}$ mice at 16 weeks and 1 year of age. The data are expressed as the mean ± SD ($Hras^{+/+}$ (n = 5) and $Hras^{G12S/+}$ (n = 7) at 16 weeks of age; $Hras^{+/+}$ (n = 5) and $Hras^{G12S/+}$ (n = 7) at 1 year of age). $^{**}p < 0.01$ (Tukey's test) compared with $Hras^{+/+}$ mice at 16 weeks and 1 year of age. $^{\#\#}p < 0.01$ (Tukey's test) compared with $Hras^{G12S/+}$ mice at 16 weeks of age. Scale bar = 50 μm. (h) Gross morphology of kidneys from $Hras^{+/+}$ and $Hras^{G12S/+}$ mice at 1 year of age. The bar graph indicates the kidney weight (KW) to body weight (BW) ratios of $Hras^{+/+}$ and $Hras^{G12S/+}$ mice at 16 weeks and 1 year of age. The data are expressed as the mean ± SD ($Hras^{+/+}$ (n = 8) and $Hras^{G12S/+}$ (n = 8) at 16 weeks of age; $Hras^{+/+}$ (n = 10) and $Hras^{G12S/+}$ (n = 7) at 1 year of age). $^{**}p < 0.01$ (Welch's *t*-test) compared with $Hras^{+/+}$ mice. Scale bar = 5 mm. (i and j) Coronal sections of kidneys from $Hras^{+/+}$ and $Hras^{G12S/+}$ mice at 1 year of age stained with HE, PAS and Sirius red. Scale bar = 100 μm. (j) The box plot shows the proportion of fibrosis area in Sirius red-stained sections ($Hras^{+/+}$ (n = 9) and $Hras^{G12S/+}$ (n = 8)). The open circle (○) indicates an outlier. $^{*}p < 0.05$ (Mann-Whitney *U* test) compared with $Hras^{+/+}$ mice. (K) Gross morphology of a cystic kidney from a $Hras^{G12S/+}$ mouse at 16 weeks of age.

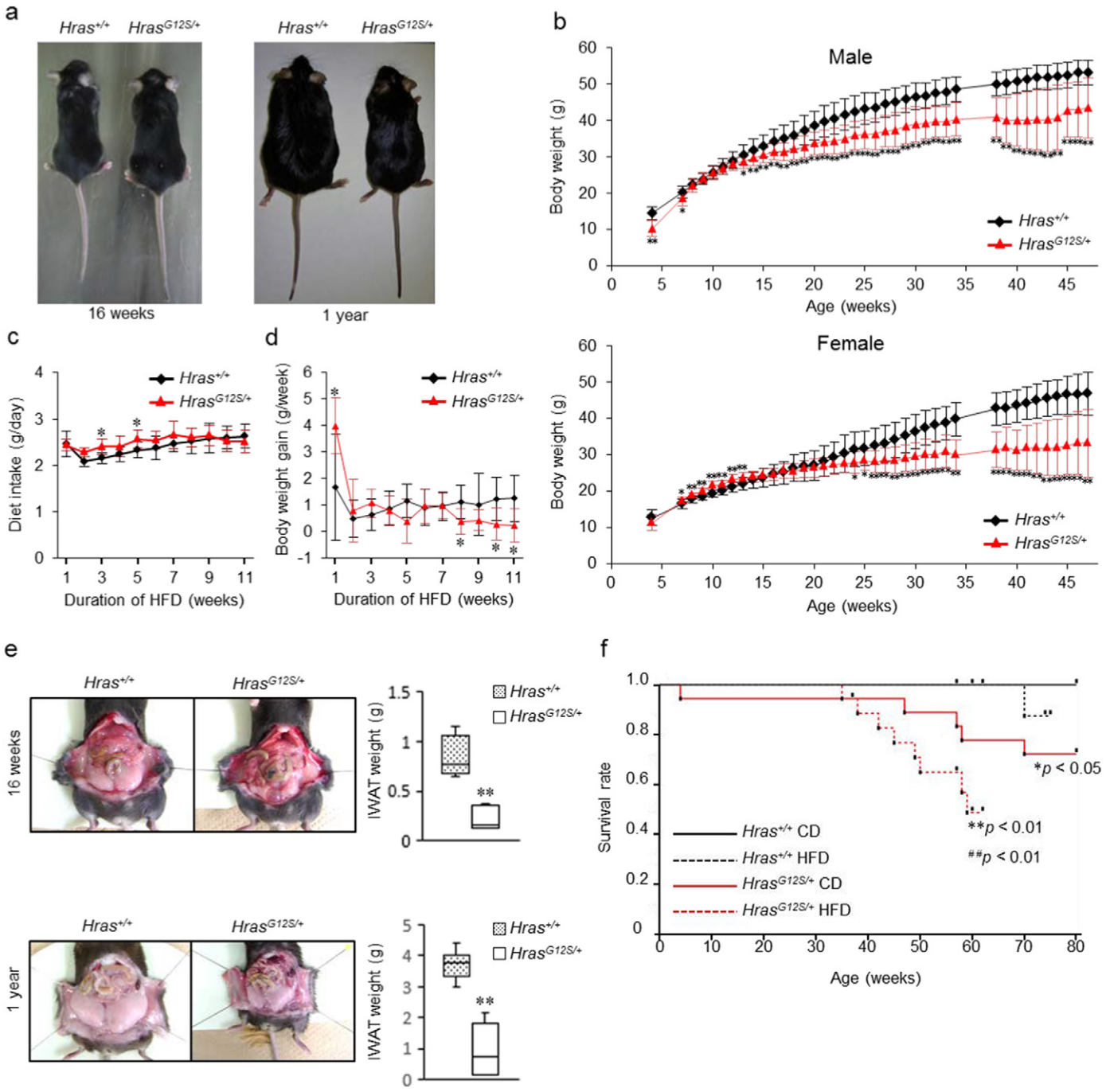

Fig. 2. Resistance to HFD-induced obesity in $Hras^{G12S/+}$ mice. (a) Representative appearance of $Hras^{+/+}$ and $Hras^{G12S/+}$ mice fed a HFD at 16 weeks and 1 year of age. (b) Body weights of $Hras^{+/+}$ and $Hras^{G12S/+}$ mice fed a HFD. The data are expressed as the mean ± SD ($Hras^{+/+}$ (n = 17) and $Hras^{G12S/+}$ (n = 18)). $^{*}p < 0.05$, $^{**}p < 0.01$ (Welch's *t*-test) compared with $Hras^{+/+}$ mice. (c and d) Food intake and body weight gain in $Hras^{+/+}$ and $Hras^{G12S/+}$ mice fed a HFD from 5 to 16 weeks of age. The data are expressed as the mean ± SD ($Hras^{+/+}$ (n = 7) and $Hras^{G12S/+}$ (n = 7)). $^{*}p < 0.05$ (Welch's *t*-test) compared with $Hras^{+/+}$ mice. (e) Representative appearance of inguinal white adipose tissue (IWAT) and IWAT weight in $Hras^{+/+}$ and $Hras^{G12S/+}$ mice fed a HFD at 16 weeks and 1 year of age ($Hras^{+/+}$ (n = 8) and $Hras^{G12S/+}$ (n = 5)). $^{*}p < 0.05$ (Mann-Whitney *U*-test) compared with $Hras^{+/+}$ mice. (f) Survival rates of $Hras^{+/+}$ and $Hras^{G12S/+}$ mice fed a CD or a HFD ($Hras^{+/+}$ CD (n = 13) and $Hras^{G12S/+}$ CD (n = 18); $Hras^{+/+}$ HFD (n = 17) and $Hras^{G12S/+}$ HFD (n = 18)). $^{*}p < 0.05$, $^{**}p < 0.01$ (log-rank test) compared with $Hras^{+/+}$ CD mice; $^{\#\#}p < 0.01$ (log-rank test) compared with $Hras^{+/+}$ HFD mice.

2.7. Blood Acylcarnitine Profiling

Mice were fed a HFD from 5 to 22–27 weeks of age. Blood samples were obtained from tail vein after 24 h of fasting and spotted on filter paper. The samples were prepared as previously described (Kobayashi et al., 2007). Blood acylcarnitine was measured using an API 3000 triple quadrupole tandem mass spectrometer along with a SIL-HTc autosampler (Shimadzu, Kyoto, Japan) and analyzed using ChemoView™ software (Applied Biosystems/MDS SCIEX, Toronto, Canada).

2.8. Urinary β-Hydroxybutyric Acid and Pyruvic Acid Measurement

Mice were fed a HFD from 5 to 22–27 weeks of age. Urine samples were blotted to filter paper then dried at room temperature. β-hydroxybutyric acid and pyruvic acid were measured by GC/MS.

Table 1
Biochemical parameters in $Hras^{+/+}$ and $Hras^{G12S/+}$ mice in fed or fasted state.

	Fed		Fasted	
	$Hras^{+/+}$	$Hras^{G12S/+}$	$Hras^{+/+}$	$Hras^{G12S/+}$
TP (g/dl)	5.0 ± 0.2	4.9 ± 0.2	5.0 ± 0.2	4.9 ± 0.2
Alb (g/dl)	3.6 ± 0.2	3.4 ± 0.2	3.6 ± 0.2	3.4 ± 0.2
BUN (mg/dl)	26.2 ± 5.7	21.4 ± 5.8	17.5 ± 5.4	18.2 ± 3.3
Creatinine (mg/dl)	0.1 ± 0.02	0.1 ± 0.02	0.2 ± 0.04	0.1 ± 0.02
UA (mg/dl)			2.9 ± 0.8	3.5 ± 0.4
Amy (IU/l)			2115.1 ± 391.3	1931.0 ± 119.8
AST (IU/l)	45.6 ± 6.3	51.0 ± 7.1	96.4 ± 21.0	77.8 ± 29.8
ALT (IU/l)	18.2 ± 2.8	19.6 ± 4.7	50.0 ± 26.7	35.8 ± 20.4
TG (mg/dl)	67.2 ± 59.8	34.2 ± 13.6	29.4 ± 13.4	41.8 ± 27.9
Total Cho (mg/dl)	98.6 ± 12.1	94.0 ± 15.2	99.0 ± 13.9	73.0 ± 10.7
F-Cho (mg/dl)	20.2 ± 2.8	20.8 ± 3.8	20.6 ± 2.6	13.4 ± 5.4$^{\#}$
E-Cho (mg/dl)	78.4 ± 10.4	73.2 ± 11.9	78.4 ± 12.2	59.6 ± 6.8
LDL-Cho (mg/dl)	6.8 ± 1.3	10.6 ± 1.8*	6.4 ± 2.3	6.0 ± 1.4$^{\#\#}$
HDL-Cho (mg/dl)	52.0 ± 7.1	46.6 ± 7.6	45.8 ± 4.8	37.8 ± 4.6
NEFA (μEq/l)	783.6 ± 343.9	647.2 ± 73.5	909.6 ± 197.3	1066.4 ± 170.3$^{\#}$
Total Bil (mg/dl)	0.1 ± 0.03	0.1 ± 0.07	0.1 ± 0.02	0.1 ± 0.02
TBA (μmol/l)	5.8 ± 6.3	14.8 ± 23.1	9.4 ± 5.5	9.4 ± 3.8
Insulin (ng/ml)	0.5 ± 0.2	0.4 ± 0.2		
Leptin (ng/ml)	12.2 ± 6.6	6.0 ± 3.8		

The mice were fed a HFD from 5 to 16 weeks of age. Blood samples were obtained using the protocol (Supplementary Fig. 5). The data are expressed as the mean ± SD. ($Hras^{+/+}$ (n = 5) and $Hras^{G12S/+}$ (n = 5) in fed state. $Hras^{+/+}$ (n = 5) and $Hras^{G12S/+}$ (n = 5) in fasted state.) Significantly different than $Hras^{+/+}$ in each fed and fasted conditons, $^{*}p < 0.05$ (Tukey's test). Significantly different than fed condition in each $Hras^{+/+}$ and $Hras^{G12S/+}$ groupes, $^{\#}p < 0.05$, $^{\#\#}p < 0.01$ (Tukey's test).

The procedures of sample preparation and measurement were as previously described (Fu et al., 2000; Kimura et al., 1999).

2.9. Histology and Immunohistochemistry

Tissues were fixed in 10% neutral buffered formalin and then embedded in paraffin. The sections were stained with hematoxylin and eosin (HE), periodic acid-Schiff (PAS) or picrosirius red. To measure the cross-sectional areas of the cardiomyocytes, the sections were stained with fluorescein isothiocyanate-labeled wheat germ agglutinin (FITC-WGA, L4895; Sigma-Aldrich, St Louis, MO) for 1 h at room temperature. The slides were mounted using the ProLong Gold antifade reagent with 4′,6-diamidino-2-phenylindole. The areas of the cardiomyocytes with nuclei were measured using ImageJ software (http://rsbweb.nih.gov/ij/).

2.10. Quantitative RT-PCR

Total RNA extraction and cDNA synthesis were performed as previously described (Inoue et al., 2014). Quantitative PCR analysis was performed using the Universal Probe Library (Roche Life Science, Basel, Switzerland) with StepOnePlus (Thermo Fisher Scientific). Amplification primers and hydrolysis probes are described in Supplementary Table 4.

2.11. Western Blotting

Liver tissues were homogenized in lysis buffer (10 mM Tris-HCL, pH 8.0 and 1% SDS) containing phosphatase and protease inhibitor cocktails (P5726 and P8340, respectively; Sigma-Aldrich). These lysates were centrifuged at 15,000 rpm for 30 min at 20° C, and the protein concentration was determined using the Bradford method with the Bio-Rad Protein Assay (Bio-Rad Laboratories, Hercules, CA). The lysates were subjected to SDS-PAGE electrophoresis (4–20% Criterion TGX Precast Gels; Bio-Rad Laboratories) and transferred to either a nitrocellulose or PVDF membrane (Trans-Blot Turbo Transfer pack; Bio-Rad Laboratories) using the Trans-Blot Turbo Transfer System (Bio-Rad Laboratories). After blocking with 5% non-fat milk, the membranes were incubated overnight at 4° C with following antibodies (the catalog numbers are in parentheses). H-Ras (sc-520) and AMPKα 1/2 (sc-25,792) from Santa Cruz Biotechnology (Santa Cruz, CA) and ERK1/2 (9102), phospho-ERK1/2 (9101), AKT (9272), phospho-AKT (on Ser473; 9018), phospho-AMPKα (on Thr172; 2535) from Cell Signaling (Danvers, MA). All of the membranes were visualized using the Western Lightning ECL-Plus Kit (PerkinElmer, Waltham, MA). The band intensities were quantified using ImageJ software.

2.12. Intraperitoneal Glucose Tolerance Test (IPGTT)

Mice were fed a HFD from 5 to 16 weeks of age before IPGTT. 2 g/kg body weight of glucose was injected intraperitoneally in mice after 6 h fasting. Blood glucose levels were measured before glucose injection and after 30, 60, 90 and 120 min of glucose injection. Samples were obtained from the tail veins of anesthetized mice and analyzed using a FreeStyle Precision Neo (Abbott Laboratories).

2.13. Statistical Analysis

The data are presented as the mean ± standard deviation (SD). The Mann-Whitney *U*-test and Welch's *t*-test were used for comparisons of

Fig. 3. Hepatic microvesicular steatosis in $Hras^{G12S/+}$ mice fed a HFD. (a) Representative gross morphology of livers from $Hras^{+/+}$ and $Hras^{G12S/+}$ mice fed a HFD at 1 year of age. (b) Crude liver weight (left bar graph) and liver weight (LW) to body weight (BW) ratio (right bar graph) of $Hras^{+/+}$ and $Hras^{G12S/+}$ mice fed a CD or HFD at 1 year of age. The data are expressed as the mean ± SD ($Hras^{+/+}$ (n = 11) and $Hras^{G12S/+}$ (n = 8) for CD-fed mice; $Hras^{+/+}$ (n = 8) and $Hras^{G12S/+}$ (n = 8) for HFD-fed mice). (c) HE-stained liver sections from $Hras^{+/+}$ and $Hras^{G12S/+}$ mice fed a HFD at 1 year of age. The arrows and arrowheads indicate macrovesicular and microvesicular lipid drops, respectively. Scale bars = 100 μm (upper panel) and 50 μm (lower panel). (d) HE-stained liver sections from $Hras^{+/+}$ and $Hras^{G12S/+}$ mice fed a HFD under fed or fasted conditions at 16 weeks of age. Samples were obtained using the described protocol (Supplementary Fig. 5). Scale bar = 50 μm. (e–h) Samples were obtained according to the described protocol (Supplementary Fig. 5). Total lipid (e), triglyceride (f), total cholesterol (g) and free fatty acid (h) levels in the liver from fed or fasted $Hras^{+/+}$ and $Hras^{G12S/+}$ mice. The data are expressed as the mean ± SD ($Hras^{+/+}$ (n = 5) and $Hras^{G12S/+}$ (n = 6) in the fed condition; $Hras^{+/+}$ (n = 6) and $Hras^{G12S/+}$ (n = 6) in the fasted condition). $^{**}p < 0.01$ (Welch's *t*-test) compared with fed $Hras^{+/+}$ and $Hras^{G12S/+}$ mice. (i-k) Blood glucose (i), urinary β-hydroxybutyric acid (j) and blood β-hydroxybutyric acid (k) levels in $Hras^{+/+}$ and $Hras^{G12S/+}$ mice. Blood and urinary samples were obtained as described (Supplementary Fig. 5). The data are expressed as the mean ± SD ($Hras^{+/+}$ (n = 7) and $Hras^{G12S/+}$ (n = 6) in the blood samples; $Hras^{+/+}$ (n = 7) and $Hras^{G12S/+}$ (n = 7) in the urinary samples). $^{*}p < 0.05$, $^{**}p < 0.01$ (Welch's *t*-test) compared with $Hras^{+/+}$ mice.

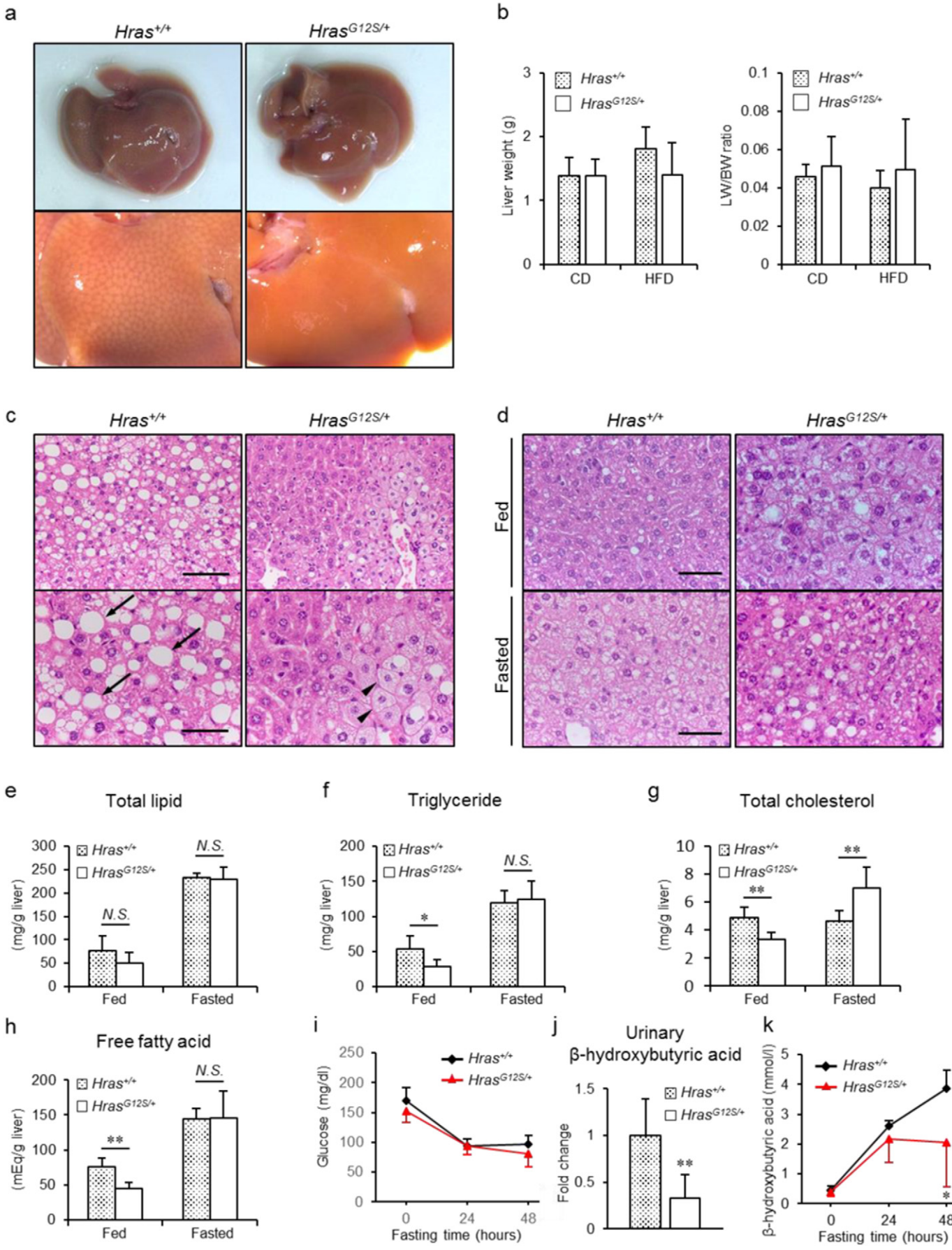
a
Hras+/+
HrasG12S/+
b
Liver weight (g)
LW/BW ratio
Hras+/+
HrasG12S/+
CD
HFD
c
d
Fed
Fasted
e
Total lipid
(mg/g liver)
N.S.
f
Triglyceride
*
g
Total cholesterol
**
h
Free fatty acid
(mEq/g liver)
i
Glucose (mg/dl)
Fasting time (hours)
j
Urinary
β-hydroxybutyric acid
Fold change
k
β-hydroxybutyric acid (mmol/l)

two groups, and Tukey's test was used for multiple comparisons. The log-rank test was used for the survival curve, which was constructed using the Kaplan-Meier method. All data were analyzed using JMP Pro12 software (SAS, Cary, NC), and $p < 0.05$ was considered statistically significant.

3. Results

3.1. Generation of Hras G12S Knock-in Mice

To generate *Hras* G12S knock-in mice, a targeting vector with a GGA (Gly) to AGC (Ser) mutation in codon 12 (Fig. 1a) was electroporated into C57B6-derived ES cells. The targeted clones were confirmed by Southern blotting (data not shown). Screened ES cells were microinjected into BALB/c blastocysts. To obtain $Hras^{G12S/+}$;*Cre* mice, the chimeras ($Hras^{G12S\ Neo/+}$ mice) were crossed with CAG-Cre transgenic mice. Male $Hras^{G12S/+}$;*Cre* mice were crossed with female C57BL/6J mice to remove Cre, and the genotype was confirmed by PCR (Supplementary Fig. 1). $Hras^{G12S/+}$ mice were present at the expected Mendelian ratios at weaning and were fertile. In contrast, all of the homozygous *Hras* G12S knock-in mice died during the prenatal period (data not shown).

3.2. $Hras^{G12S/+}$ Mice Exhibit Facial Dysmorphia, Growth Alterations, Cardiomyocyte Hypertrophy and Kidney Anomalies

Patients with Costello syndrome have postnatal onset of growth deficiency associated with feeding difficulty; several facial features, including macrocephaly with a prominent forehead, low-set ears with thick lobes, strabismus, a depressed nasal bridge, thick lips, curly hair and dental anomalies; cardiac anomalies; skin anomalies and renal anomalies (Hennekam, 2003; Myers et al., 2014; Takahashi and Ohashi, 2013). All $Hras^{G12S/+}$ mice exhibited dysmorphic facial features, including a round head and a shortened nasal bridge (Fig. 1b). These facial features were reminiscent of the *Hras* G12V knock-in mouse (Chen et al., 2009; Schuhmacher et al., 2008). In addition, malocclusion and rectal prolapse were observed in $Hras^{G12S/+}$ mice (Fig. 1c and d; Supplementary Table 5). Skin anomalies and curly hair were not observed in $Hras^{G12S/+}$ mice. Both male and female 5-week-old $Hras^{G12S/+}$ mice displayed significant growth retardation, although the body weights of these mice normalized by 6 weeks of age (Fig. 1e). Thereafter, the female, but not male, $Hras^{G12S/+}$ mice displayed significant overgrowth after 9 weeks of age compared with $Hras^{+/+}$ mice (Fig. 1e).

The representative cardiac anomalies in Costello syndrome are arrhythmia, hypertrophic cardiomyopathy, atrial septal defects and ventricular septal defects (Hennekam, 2003). $Hras^{G12S/+}$ mice had cardiomegaly, which was characterized by a significantly increased heart weight (HW) to body weight (BW) ratio compared with $Hras^{+/+}$ mice (Fig. 1f). Morphometric analysis of left ventricular (LV) cardiomyocytes indicated that these cells were significantly larger in $Hras^{G12S/+}$ mice than in $Hras^{+/+}$ mice; this cellular enlargement progressed over time but did not result in the development of cardiac fibrosis (Fig. 1g and Supplementary Fig. 2). At 1 year of age, electrocardiographic analysis revealed significantly deep S waves, low T waves and a short PR interval in $Hras^{G12S/+}$ mice compared with $Hras^{+/+}$ mice (Supplementary Table 6). Despite the cardiomegaly and cardiomyocyte hypertrophy, there were no significant changes in intraventricular septum thickness or left ventricular systolic function, including ejection fraction and fractional shortening on echocardiograms, in $Hras^{G12S/+}$ mice compared with $Hras^{+/+}$ mice at 1 year of age. These results suggest that there were no significant changes in cardiac function (Supplementary Table 7). Furthermore, the heart structure of $Hras^{G12S/+}$ mice appeared normal in the echocardiographic and histological analyses, suggesting that there were no atrial septal defects or ventricular septal defects (data not shown). A significantly increased kidney weight (KW) to BW ratio, mesangial proliferation and kidney fibrosis indicated renal enlargement in $Hras^{G12S/+}$ mice at 1 year of age (Fig. 1h-1j) but not at 16 weeks of age (data not shown). Furthermore, 4.6% of the $Hras^{G12S/+}$ mice had a unilateral cystic kidney (Fig. 1k; Supplementary Table 5). These observations indicate that $Hras^{G12S/+}$ mice have dysmorphic facial features, overgrowth (in females), cardiomegaly with cardiomyocyte hypertrophy and kidney anomalies.

3.3. $Hras^{G12S/+}$ Mice Are Resistant to HFD-Induced Weight Gain

Because we did not observe any differences in body weight between $Hras^{+/+}$ and $Hras^{G12S/+}$ mice on a normal diet, we used a model of HFD-induced obesity to explore the metabolic status of $Hras^{G12S/+}$ mice. Male $Hras^{G12S/+}$ mice were significantly lighter than $Hras^{+/+}$ mice after 13 weeks of age with HFD feeding. In female mice, there were no differences in body weight between $Hras^{+/+}$ and $Hras^{G12S/+}$ mice from 14 to 23 weeks of age. After 24 weeks of age, $Hras^{G12S/+}$ mice were significantly lighter than $Hras^{+/+}$ mice (Fig. 2a and b). Food intake from birth to 11 weeks was comparable between $Hras^{+/+}$ and $Hras^{G12S/+}$ mice, except during the third and fifth weeks of HFD feeding (Fig. 2c); during these weeks, food intake by $Hras^{G12S/+}$ mice was significantly higher than that by $Hras^{+/+}$ mice (Fig. 2c). The average weight gain of $Hras^{G12S/+}$ mice was significantly lower than that of $Hras^{+/+}$ mice after 8 weeks but not after 9 weeks, despite the increased or comparable levels of food intake by $Hras^{G12S/+}$ mice (Fig. 2d). Furthermore, there was less inguinal white adipose tissues in $Hras^{G12S/+}$ mice at both 16 weeks and 1 year of age compared with $Hras^{+/+}$ mice (Fig. 2e). A dramatic increase in mortality was observed among $Hras^{G12S/+}$ mice fed a HFD compared with $Hras^{G12S/+}$ mice fed a CD, whereas $Hras^{G12S/+}$ mice were resistant to HFD-induced obesity (Fig. 2f). Consistent with the increased mortality of HFD-fed $Hras^{G12S/+}$ mice, $Hras^{G12S/+}$ mice developed progressive cardiomyocyte hypertrophy and kidney injury (Supplementary Fig. 3). Furthermore, the $Hras^{G12S/+}$ mice that died at 60 weeks of age had developed the aging phenotype, including hair loss, kyphosis and cutaneous lesions due to scratching (data not shown). These phenotypes, including increased mortality, cardiomyocyte hypertrophy and kidney injury, were more pronounced in female $Hras^{G12S/+}$ mice than in male $Hras^{G12S/+}$ mice (data not shown). Thus, a subsequent study was performed using female $Hras^{G12S/+}$ mice.

3.4. $Hras^{G12S/+}$ Mice Fed a HFD Exhibit Impaired Fatty Acid Oxidation

Since $Hras^{G12S/+}$ mice were resistant to HFD-induced obesity, we conducted a biochemical analysis of the blood and liver to examine the metabolic status of these mice. Serum LDL cholesterol levels were significantly higher in $Hras^{G12S/+}$ mice fed a HFD than in $Hras^{+/+}$ mice fed a HFD (Table 1). However, there were no differences in the other parameters. Gross observation of the livers revealed a yellowish, steatotic appearance in the 1-year-old $Hras^{+/+}$ mice, whereas $Hras^{G12S/+}$ mouse livers were normal (Fig. 3a). There were no significant differences in liver weight between the $Hras^{+/+}$ and $Hras^{G12S/+}$ mice that were fed either a HFD or a CD (Fig. 3b). The 1-year-old $Hras^{+/+}$ mice fed a HFD exhibited hepatic steatosis with macrovesicular lipid droplets, whereas the corresponding $Hras^{G12S/+}$ mice exhibited hepatic steatosis with microvesicular lipid droplets (Fig. 3c). Hepatic steatosis with microvesicular lipid droplets was already evident in $Hras^{G12S/+}$ mice that had been fed a HFD for 11 weeks (Supplementary Fig. 4).

Hepatic steatosis with microvesicular lipid droplets, which indicates fatty acid accumulation, is observed in cases of mitochondrial injury and impaired mitochondrial fatty acid oxidation (such as in Reye syndrome) (Fromenty et al., 1997; Fromenty and Pessayre, 1997). Under starvation conditions, patients with impaired mitochondrial fatty acid oxidation are not able to utilize fatty acids in the liver, which leads to increased free fatty acid levels in the blood, lipid accumulation in the liver, and decreased ketone body production (Vishwanath, 2016). To elucidate if the hepatic steatosis with microvesicular lipid droplets observed in $Hras^{G12S/+}$ mice is caused by impaired mitochondrial fatty acid

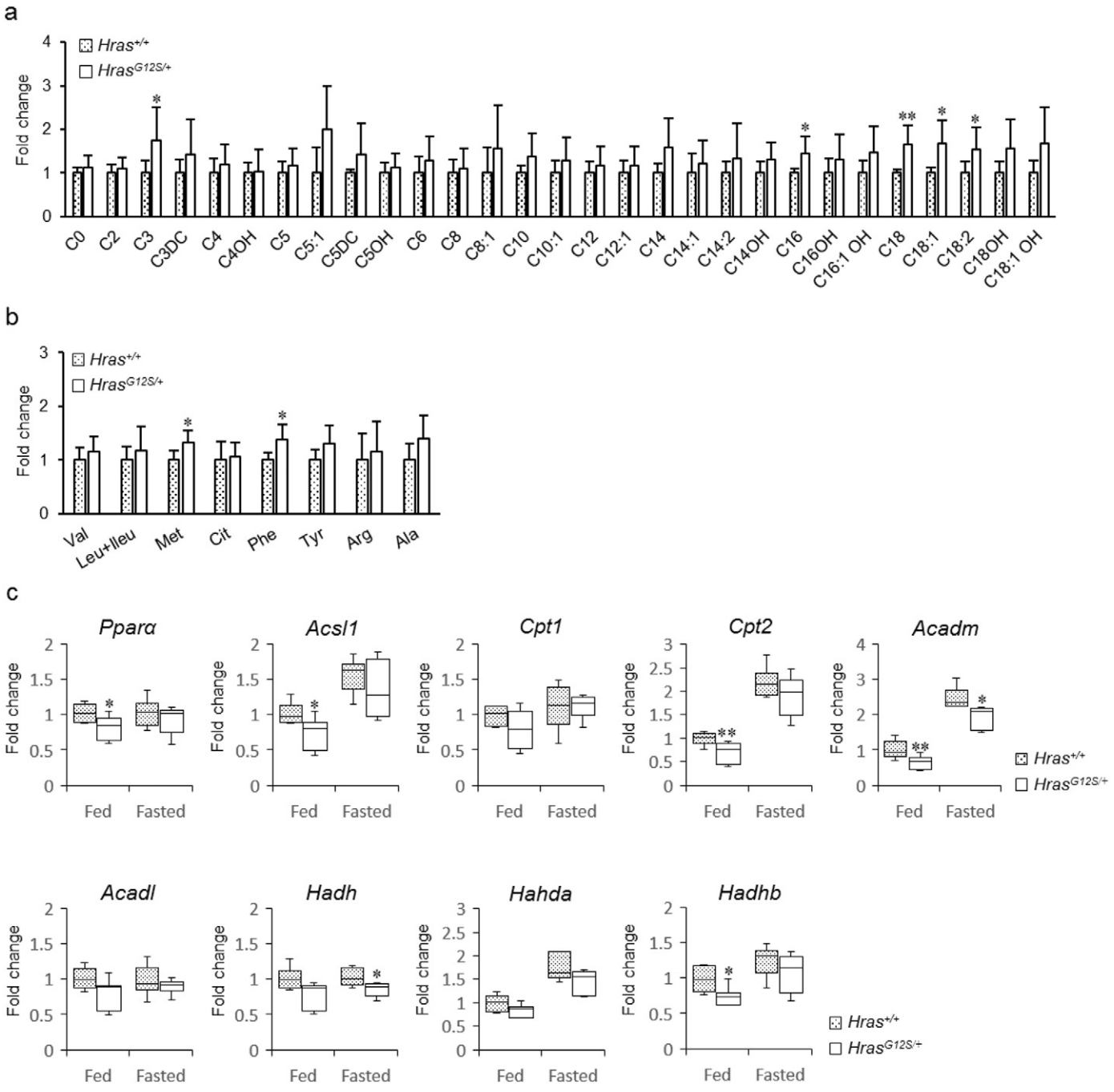

Fig. 4. Changes in parameters related to mitochondrial fatty acid oxidation in liver tissues from fed or fasted $Hras^{+/+}$ and $Hras^{G12S/+}$ mice. (a and b) Relative blood acylcarnitine (a) and amino acid (b) levels in $Hras^{+/+}$ and $Hras^{G12S/+}$ mice after 24 h of fasting. Blood samples were obtained as described (Supplementary Fig. 5). The data are expressed as the mean ± SD ($Hras^{+/+}$ (n = 7) and $Hras^{G12S/+}$ (n = 7)). *$p < 0.05$, **$p < 0.01$ (Welch's *t*-test) compared with $Hras^{+/+}$ mice. Val, valine; Leu, leucine; Ileu, Isoleucine; Met, methionine; Cit, citrulline; Phe, phenylalanine; Tyr, tyrosine; Arg, arginine; Ala, alanine. (c) Relative mRNA expression of genes related to mitochondrial β-oxidation in liver tissues from $Hras^{+/+}$ and $Hras^{G12S/+}$ mice ($Hras^{+/+}$ (n = 6) and $Hras^{G12S/+}$ (n = 7) in the fed condition; $Hras^{+/+}$ (n = 6) and $Hras^{G12S/+}$ (n = 6) in the fasted condition). Samples were obtained as described (Supplementary Fig. 5). mRNA levels of target genes were normalized to those of *Gapdh*. *$p < 0.05$,** $p < 0.01$ (Welch's *t*-test or Mann-Whitney *U*-test) compared with $Hras^{+/+}$ mice.

oxidation, we examined liver tissues, blood glucose levels, blood and urinary β-hydroxybutyric acid levels and serum biochemical parameters in fasted mice that were fed a HFD from 5 to 16 weeks of age (Supplementary Fig. 5).

Under fasted conditions, liver sections from $Hras^{G12S/+}$ mice showed the accumulation of large lipid droplets (Fig. 3d). In contrast, $Hras^{+/+}$ mice exhibited an increase in microvesicular lipid droplets in the liver. Serum non-esterified fatty acid (NEFA) levels, one free fatty acid (FFA) parameter, were significantly elevated in fasted $Hras^{G12S/+}$ mice compared with non-fasted mice. In contrast, serum NEFA levels in $Hras^{+/+}$ mice were comparable in fed and fasted conditions (Table 1). The hepatic levels of total cholesterol, triglycerides and free fatty acids were lower in $Hras^{G12S/+}$ mice than in $Hras^{+/+}$ mice on a HFD. However, under fasted conditions, the lipid content (including triglycerides, total cholesterol and free fatty acids) in the liver of $Hras^{G12S/+}$ mice increased to the same levels as those in $Hras^{+/+}$ mice. These liver histology and lipid content results (Fig. 3e-3h) suggested decreased FFA utilization in the liver of $Hras^{G12S/+}$ mice in the fasted condition.

The blood glucose levels were comparable in $Hras^{G12S/+}$ mice and $Hras^{+/+}$ mice during 48 h of fasting (Fig. 3i). Urinary β-hydroxybutyric acid levels after 24 h of fasting were significantly lower in $Hras^{G12S/+}$ mice than in $Hras^{+/+}$ mice (Fig. 3j). Thereafter, blood β-hydroxybutyric

acid levels were significantly reduced in $Hras^{G12S/+}$ mice after 48 h of fasting (Fig. 3k), suggesting decreased ketone body production. A line of evidence suggests that under fasted conditions, $Hras^{G12S/+}$ mice fed a HFD develop impaired fatty acid oxidation, including decreased lipid utilization in the liver, elevated levels of NEFA and hypoketosis.

3.5. $Hras^{G12S/+}$ Mice Fed a HFD Exhibit an Increase in Long-Chain Fatty Acylcarnitines

Impaired mitochondrial fatty acid oxidation leads to hypercatabolism and an increase in various types of fatty acylcarnitines in the blood under starvation conditions (Vishwanath, 2016). After 24 h of fasting, tandem mass spectrometry analysis of blood acylcarnitine profiles showed a significant increase in long-chain fatty acylcarnitines, including C16, C18, C18:1 and C18:2, in $Hras^{G12S/+}$ mice fed a HFD (Fig. 4a), suggesting decreased activity of an earlier step in mitochondrial fatty acid oxidation. In the blood amino acid profiles, the methionine and phenylalanine levels were significantly higher in $Hras^{G12S/+}$ mice than in $Hras^{+/+}$ mice (Fig. 4b), suggesting hypercatabolism.

In addition, we evaluated the mRNA expression of genes related to mitochondrial fatty acid oxidation. In the fed condition, the hepatic mRNA expression of peroxisome proliferator-activated receptor alpha (*Pparα*), acyl-CoA synthetase long-chain family member 1 (*Acsl1*), carnitine palmitoyltransferase 2 (*Cpt2*), medium-chain acyl-CoA dehydrogenase (*Acadm*) and mitochondrial trifunctional enzyme subunit beta (*Hadhb*) was significantly lower in $Hras^{G12S/+}$ mice than in $Hras^{+/+}$ mice (Fig. 4c). A significant decrease in *Acadm* and short-chain-3-hydroxyacyl-CoA dehydrogenase (*Hadh*) gene expression was observed in fasted $Hras^{G12S/+}$ mice compared with $Hras^{+/+}$ mice (Fig. 4c). These findings indicate that mitochondrial fatty acid oxidation is impaired in the livers of $Hras^{G12S/+}$ mice.

3.6. $Hras^{G12S/+}$ Mice Fed a HFD Exhibit Alterations in Glucose, Organic Acid and Glutamine Metabolism

We hypothesized that the introduction of the *Hras* G12S mutation *in vivo* causes metabolic changes in addition to those to fatty acid oxidation that might be similar to those observed in cancer cells (Bryant et al., 2014; Zheng et al., 2015; Zhou et al., 2016). We then performed comprehensive RT-qPCR analysis of genes involved in glucose, organic acid and glutamine metabolism in liver tissues (Supplementary Table 4). The mRNA levels of genes involved in glucose metabolism (glucose-6-phosphate dehydrogenase, *G6pd*) and glutaminolysis (aspartate aminotransferase 1, *Got1*) were significantly increased in fed and/or fasted $Hras^{G12S/+}$ mice (Fig. 5a and b). Furthermore, pyruvate dehydrogenase alpha (*Pdha*) mRNA expression was significantly decreased in fed $Hras^{G12S/+}$ mice, and glutaryl-CoA dehydrogenase (*Gcdh*), glutamate dehydrogenase 1 (*Glud1*) and malic enzyme 1 (*Me1*) mRNA levels were decreased in both fed and fasted $Hras^{G12S/+}$ mice (Fig. 5a-5c). To evaluate the differences in glucose metabolism between $Hras^{+/+}$ and $Hras^{G12S/+}$ mice, we performed an intraperitoneal glucose tolerance test (IPGTT) and measured urinary pyruvic acid. $Hras^{G12S/+}$ mice displayed significantly lower blood glucose levels than $Hras^{+/+}$ mice after 30 min in the IPGTT (Fig. 5d). Moreover, $Hras^{G12S/+}$ mice fed a CD showed significantly lower blood glucose levels after 30 min of fasting. $Hras^{G12S/+}$ mice fed a HFD also had significantly lower blood glucose levels after 90 min of fasting (Supplementary Fig. 6a). Under these conditions, blood insulin levels after 90 min of fasting were comparable between $Hras^{+/+}$ and $Hras^{G12S/+}$ mice (Supplementary Fig. 6b). Urinary pyruvic acid levels after 24 h of fasting were significantly higher in $Hras^{G12S/+}$ mice than in $Hras^{+/+}$ mice (Fig. 5e). These results suggest that $Hras^{G12S/+}$ mice fed a HFD show changes in glucose, organic acid and glutamine metabolism and indicate that fasting leads to insulin-independent early hypoglycemia and enhanced glutaminolysis.

We also performed western blotting to elucidate the signaling pathways altered in the $Hras^{G12S/+}$ mouse liver. Phosphorylated ERK levels in the livers of $Hras^{+/+}$ and $Hras^{G12S/+}$ mice showed no significant differences under the fed condition (Supplementary Fig. 7). In contrast, the hepatic levels of phosphorylated ERK were significantly higher in fasted $Hras^{G12S/+}$ mice than in fasted $Hras^{+/+}$ mice (Fig. 5f). There were no significant differences between the $Hras^{+/+}$ and $Hras^{G12S/+}$ mice in the levels of phosphorylated AKT (Ser 473), which is activated by RAS signaling, or of phosphorylated AMPK (Thr 172), which is associated with fatty acid and glycogen metabolism and cell growth (Carling, 2004; Hardie, 2004) (Fig. 5f).

4. Discussion

In this study, we generated heterozygous *Hras* G12S knock-in mice as a mouse model of Costello syndrome to explore the implications of germline *HRAS* activation *in vivo* on metabolic homeostasis. $Hras^{G12S/+}$ mice fed a HFD exhibited poor weight gain, decreased fatty acid oxidation and altered metabolism of glucose, organic acids and glutamine in the liver. Impaired fatty acid oxidation, hypoketosis and insulin-independent early hypoglycemia were clearly evident under fasted conditions after HFD feeding. Taken together, our results demonstrate that knock-in mice expressing germline *Hras* G12S exhibit impaired hepatic energy homeostasis when fed a HFD.

Our investigation revealed that $Hras^{G12S/+}$ mice fed a HFD exhibit microvesicular steatosis with decreased mRNA levels of genes involved in fatty acid oxidation, suggesting impaired mitochondrial function and mitochondrial fatty acid oxidation. Furthermore, increased lipid accumulation in the liver, blood methionine and phenylalanine levels, and long-chain fatty acylcarnitines, including C16, C18, C18:1 and C18:2, and decreased ketone body and blood glucose levels were observed in fasted $Hras^{G12S/+}$ mice. Abnormal accumulation of long-chain fatty acylcarnitines, including C12–18, is observed in patients with mitochondrial trifunctional protein (*MTP*), *CPT2* and carnitine-acylcarnitine translocase (*CACT*) deficiencies (Hori et al., 2010; Olpin et al., 2005; Rubio-Gozalbo et al., 2004). Biallelic *Mtp* knockout mice have been shown to exhibit microvesicular hepatic steatosis, neonatal hypoglycemia, sudden death and elevations of C14, C16, C16:1, C18:1 and C18:2 acylcarnitines, whereas heterozygous *Mtp* knockout mice do not show hypoglycemia (Ibdah et al., 2001). A recent publication on liver-specific *Cpt2* knockout mice reported microvesicular hepatic steatosis and significantly low levels of serum β-hydroxybutyric acid without hypoglycemia (Lee et al., 2016). Moreover, recent studies have reported mitochondrial dysfunction in both HRAS-transformed cells and patients with RASopathies (Aeby et al., 2007; Biaglow et al., 1997; Kleefstra et al., 2011; Telang et al., 2007; Yang et al., 2010). It is possible that impaired mitochondrial fatty acid oxidation is associated with hypoglycemia,

Fig. 5. Changes in hepatic gene expression related to glucose, organic acid and glutamine metabolism and glucose and pyruvic acid utilization in fed or fasted $Hras^{+/+}$ and $Hras^{G12S/+}$ mice. (a–c) Samples were obtained as described (Supplementary Fig. 5). Relative mRNA expression levels of genes related to glucose (a), glutamine (b) and organic acid (c) metabolism in liver tissues from fed or fasted $Hras^{+/+}$ and $Hras^{G12S/+}$ mice. ($Hras^{+/+}$ (n = 6) and $Hras^{G12S/+}$ (n = 7) in the fed condition; $Hras^{+/+}$ (n = 6) and $Hras^{G12S/+}$ (n = 6) in the fasted condition). mRNA levels of target genes were normalized to those of *Gapdh*. The open circle (○) indicates an outlier. $^{*}p < 0.05$, $^{**}p < 0.01$ (Welch's *t*-test or Mann-Whitney *U*-test) compared with $Hras^{+/+}$ mice. (d) IPGTT analysis of blood glucose levels in $Hras^{+/+}$ and $Hras^{G12S/+}$ mice at 16 weeks of age. The data are expressed as the mean ± SD ($Hras^{+/+}$ (n = 8) and $Hras^{G12S/+}$ (n = 5)). $^{*}p < 0.05$, $^{**}p < 0.01$ (Welch's *t*-test) compared with $Hras^{+/+}$ mice. (e) Urinary pyruvic acid levels in $Hras^{+/+}$ and $Hras^{G12S/+}$ mice ($Hras^{+/+}$ (n = 7) and $Hras^{G12S/+}$ (n = 7)). Urine samples were obtained as described (Supplementary Fig. 5). The bars indicate the mean. Statistical analysis was performed using the Mann-Whitney *U*-test. (f) Western blotting of liver tissues from fasted $Hras^{+/+}$ and $Hras^{G12S/+}$ mice. The lower bar graphs show the relative phospho-ERK and phospho-AKT levels. The band intensity was normalized to that of the non-phosphorylated protein. The data are expressed as the mean ± SD ($Hras^{+/+}$ (n = 5) and $Hras^{G12S/+}$ (n = 5)). $^{**}p < 0.01$ (Welch's *t*-test) compared with $Hras^{+/+}$ mice.

poor weight gain and cardiomyopathy in patients with Costello syndrome.

Hras$^{G12S/+}$ and *Hras*^{G12V} knock-in mice exhibited no growth retardation or feeding difficulty on the control diet (Chen et al., 2009; Schuhmacher et al., 2008). However, *Hras*$^{G12S/+}$ mice developed a lean phenotype with poor weight gain, reduced adiposity and fat malabsorption during HFD feeding. The mouse model of Noonan syndrome with multiple lentigines (LS mice) expressing a heterozygous *Ptpn11* T468M mutation exhibited resistance to HFD-induced obesity and reduced adiposity (Tajan et al., 2014), which are similar findings to

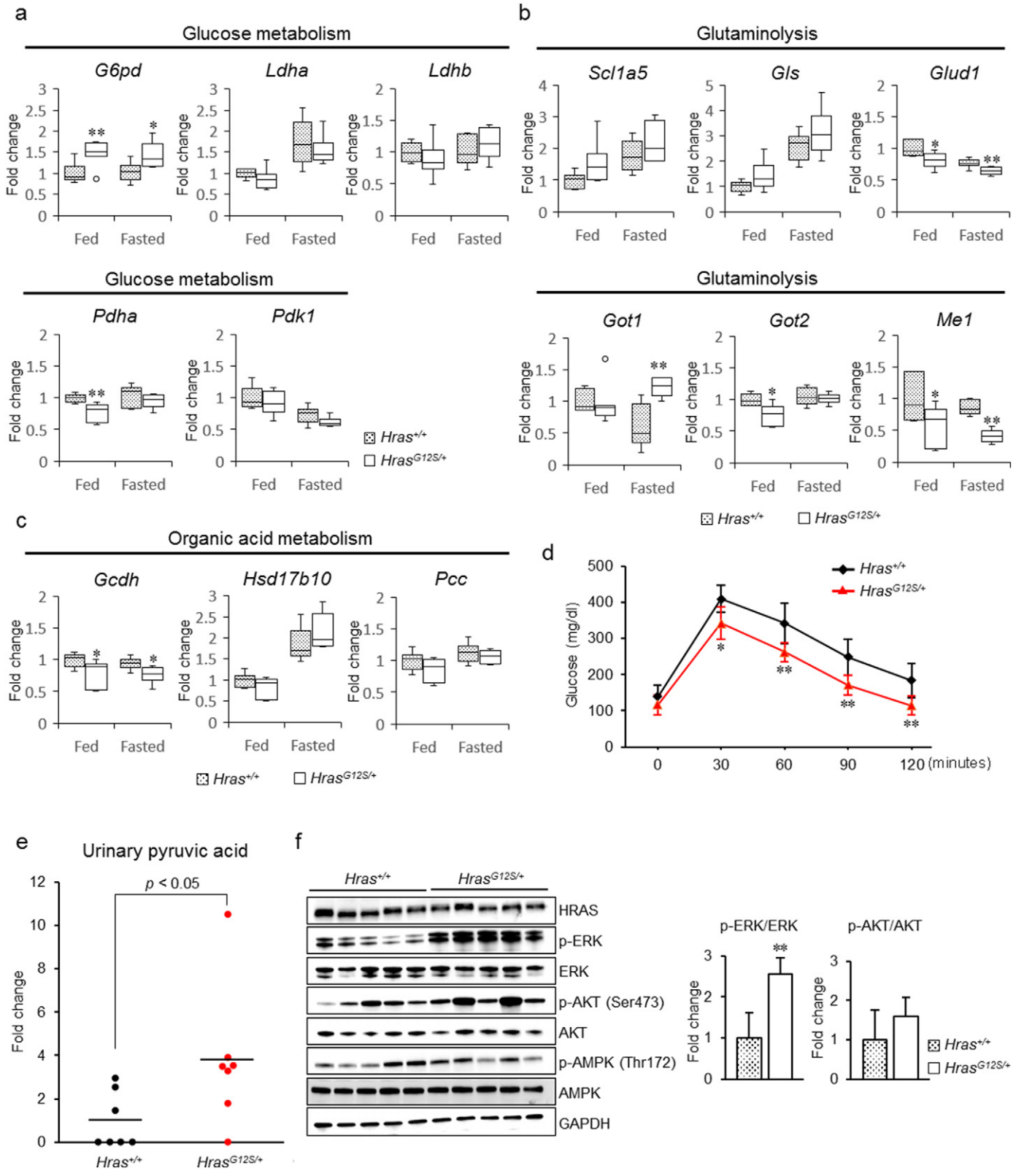

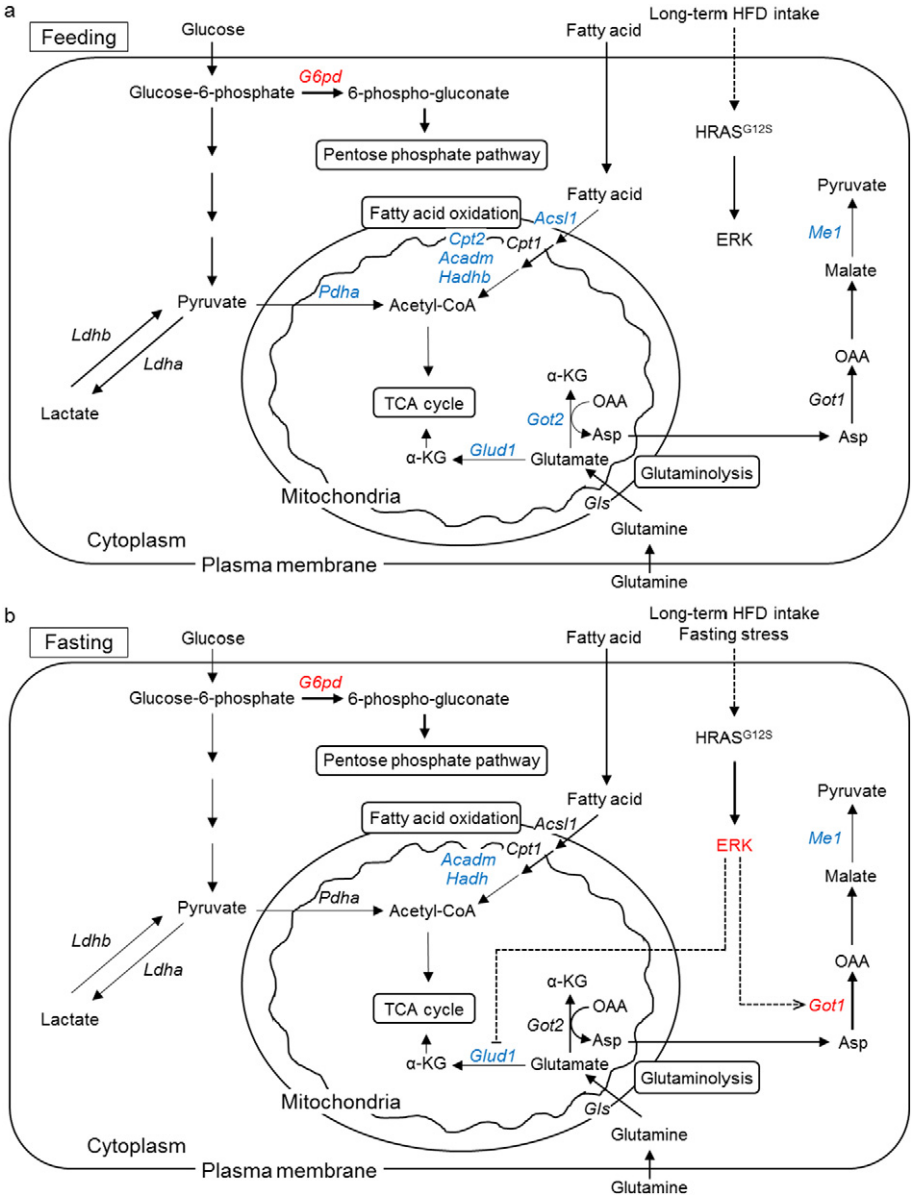

Fig. 6. Schematic of the metabolic changes in the liver of fed and fasted *Hras*$^{G12S/+}$ mice. (a and b) Changes in gene expression in the liver of *Hras*$^{G12S/+}$ mice under fed (a) and fasted (b) conditions. Upregulated or activated proteins and genes are shown in red. Decreased gene expression is shown in blue. (a) In the fed condition, the pentose phosphate pathway is activated due to an increase in *G6pd* gene expression. A decrease in *Pdha* gene expression inhibits the conversion of pyruvate to acetyl-CoA. Low *Glud1* and *Got2* gene expression results in a decrease in alpha-ketoglutaric acid. In the fatty acid oxidation pathway, decreased *Acsl1*, *Cpt2*, *Acadm* and *Hadhb* gene expression leads to a lack of acetyl-CoA. (b) In the fasted condition, the *Hras* G12S mutation leads to increased *Got1* expression and decreased *Glud1* expression through ERK activation. The *G6pd* gene is also activated in the fed condition. Upregulation of *Got1* and downregulation of *Glud1* lead to diminished levels of alpha-ketoglutaric acid, which is used to produce ATP in the TCA cycle. The reduced gene expression of *Acadm* and *Hadh* leads to impaired fatty acid oxidation, which is the main energy supplier under conditions of starvation. Gln, glutamine; Glu, glutamate; Asp, aspartic acid; OAA, oxaloacetic acid; α-KG, alpha-ketoglutaric acid.

those of our present study. Furthermore, LS mice show decreased adipogenesis, increased energy expenditure and enhanced insulin signaling. MEK inhibitors lead to increased body weight and adiposity in LS mice and increased body weight in the mouse model of Noonan syndrome and CFC syndrome (Inoue et al., 2017; Tajan et al., 2014; Wu et al., 2011). Interestingly, mouse models of CFC syndrome from our group and another group also exhibited a reduction in adiposity (Urosevic et al., 2011). A recent study showed that patients with Costello syndrome exhibit an increased energy expenditure (Leoni et al., 2016). Patients with Noonan or CFC syndrome have been shown to have intestinal lymphangiectasia, which results in fat malabsorption and growth retardation (Joyce et al., 2016; Mistilis et al., 1965; Vignes and Bellanger, 2008). Thus, these metabolic alterations, including decreased adipogenesis, fat malabsorption, lymphatic disorders, increased energy expenditure and enhanced insulin signaling, may be common in RASopathies. Future studies will increase our understanding of the mechanism behind the lean phenotype of *Hras*$^{G12S/+}$ mice fed a HFD.

Normal differentiated cells metabolize glucose to carbon dioxide through the mitochondrial tricarboxylic acid (TCA) cycle, which is the most effective way to generate ATP. In contrast, cancer cells prefer to metabolize glucose to lactate through glycolysis under aerobic conditions, which is known as “the Warburg effect” (Warburg, 1956). Several reports have suggested that the RAS oncogene promotes anaerobic glycolysis, glucose uptake, lipid synthesis and nucleotide synthesis through the pentose phosphate pathway (PPP) (Tian et al., 1998). Under both fed and fasted conditions, the metabolic alterations observed in *Hras*$^{G12S/+}$ mice (Fig. 6), including changes in glucose, organic acid and glutamine

metabolism, are similar to those in several previous reports on cancer. For example, HRAS-transformed human breast epithelial cells have been reported to have increased glycolysis and lactate production and enhanced expression of *G6pd*, which encodes a PPP regulatory enzyme (Zheng et al., 2015). Moreover, approximately 50% of diethylnitrosamine-induced liver tumors have *HRAS* mutations in codon 61, an *HRAS* hot spot in cancer. In a microarray analysis, diethylnitrosamine-induced liver tumors showed upregulation of *G6pd*, which is involved in glycolysis, and downregulation of *GCDH* and *ME1*, which are involved in organic acid and glutamine metabolism (Unterberger et al., 2014). These results were similar to the phenotype of $Hras^{G12S/+}$ mice fed a HFD (Fig. 6). Studies of pancreatic ductal adenocarcinoma with a *KRAS* mutation showed an upregulation of glycolysis-associated genes, including glucose transporter 1 (*GLUT1*), hexokinase 1 and 2 (*HK1* and *HK2*), phosphofructokinase 1 (*PFK1*) and lactate dehydrogenase A (*LDHA*) (Bryant et al., 2014; Son et al., 2013). In addition, these cancers exhibited an upregulation of *GOT1* and *GOT2* and a downregulation of *GLUD1*. These results are somewhat similar to our results, in which hepatic phosphorylated ERK levels and *Got1* expression increased in fasted $Hras^{G12S/+}$ mice after HFD feeding (Fig. 5b and f). Collectively, somatic RAS mutations and the germline *Hras* G12S mutation in mice are associated with glucose, organic acid and glutamine metabolism.

$Hras^{G12V}$ knock-in mice have been generated in two laboratories. Phenotypes between two $Hras^{G12V}$ knock-in mice were different because of the different genetic background. $Hras^{G12V}$ knock-in mice reported by Schumacher et al. showed normal weight and size, facial dysmorphia, cardiomegaly with cardiomyocyte hypertrophy, aortic valve thickening, cardiac and kidney fibrosis. However, tumor development was rare in these mice (Schuhmacher et al., 2008). In contrast, $Hras^{G12V}$ knock-in mice reported by Chen et al., showed high perinatal lethality, dysmorphic facial features, defective dental ameloblasts, malocclusion, papillomas and angiosarcomas, but did not develop any cardiac defects (Chen et al., 2009). In this study, $Hras^{G12S/+}$ mice exhibited dysmorphic facial features (including a round head and a shortened nasal bridge), a malocclusion, cardiomegaly with cardiomyocyte hypertrophy and kidney fibrosis. These phenotypes were reminiscent of the characteristic features of Costello syndrome patients and $Hras^{G12V}$ knock-in mice (Chen et al., 2009; Schuhmacher et al., 2008; Viosca et al., 2009). However, the papillomas and angiosarcomas reported in $Hras^{G12V}$ knock-in mice (Chen et al., 2009) were not observed in $Hras^{G12S/+}$ mice, even at 1 year of age. These differences are consistent with the higher cancer frequency associated with *HRAS* G12V than with *HRAS* G12S and the higher population of the GTP-bound active form of *HRAS* G12 V than *HRAS* G12S ((Wey et al., 2013) and the cosmic database). $Hras^{G12S/+}$ mice also exhibited rectal prolapse, metabolic changes, a unilateral cystic kidney and glomerulopathy, which have not been reported in $Hras^{G12V}$ knock-in mice. Although histological examination of the kidneys of patients with Costello syndrome have not been reported, ultrasonographic changes, including pelviectasis, hydronephrosis, increased kidney size and echogenic kidneys, have been observed in RASopathy patients during the perinatal period (Myers et al., 2014), suggesting a presymptomatic state of polycystic kidneys (Avni et al., 2002). Indeed, polycystic kidneys have been observed in *Hras* G12V transgenic mice (Gilbert et al., 1997; Schaffner et al., 1993). These results suggest that oncogenic *HRAS* mutations may be associated with the development of renal cysts.

Here, we developed $Hras^{G12S/+}$ mice as a model that recapitulates the pathophysiology of Costello syndrome. Our study provides evidence that individuals expressing the germline *Hras* G12S mutation could have altered energy homeostasis when consuming a HFD. Given that cells with oncogenic *RAS* mutations exhibit cancer-specific alterations in energy homeostasis, our $Hras^{G12S/+}$ mice will provide an *in vivo* model for studying cancer metabolism. Additional studies will be necessary to understand the precise mechanism of energy homeostasis in $Hras^{G12S/+}$ mice and in patients with Costello syndrome and cancer.

Acknowledgements

We wish to thank Riyo Takahashi, Kumi Kato and Yoko Tateda for technical assistance and Hiroaki Nagao and Kenji Yoshiwara for technical assistance and discussions of the experimental data. We would also like to acknowledge the support of the Biomedical Research Core of the Tohoku University Graduate School of Medicine.

Funding Sources

This work was supported by the Funding Program for the Next Generation of World-Leading Researchers (NEXT Program) from the Ministry of Education, Culture, Sports, Science and Technology of Japan to Y.A. (LS004), the Grants-in-Aid by the Practical Research Project for Rare/Intractable Diseases from the Japan Agency for Medical Research and Development, AMED to Y.A. (16eK0109021,17894363), by the Japan Society for the Promotion of Science (JSPS) KAKENHI Grant Number 26293241 and 16K15522 to Y.A., and by JSPS KAKENHI Grant Number 15K19598 to S.I.

Conflicts of Interest

There are no conflicts of interest.

Author Contributions

D.O., S.I., Y.M. and Y.A. designed the experiments and wrote the manuscript. D.O., S.I, S.M, S.T., M.M., Y.N., S.Y. and Y.A. conducted experiments. D.O., S.I, S.M., Y.N., T.N., S.Y. Y.M. and Y.A. contributed to data analysis.

Appendix A. Supplementary data

Supplementary data to this article can be found online at https://doi.org/10.1016/j.ebiom.2017.11.029.

References

Aeby, A., Sznajer, Y., Cave, H., Rebuffat, E., Van Coster, R., Rigal, O., Van Bogaert, P., 2007. Cardiofaciocutaneous (CFC) syndrome associated with muscular coenzyme Q10 deficiency. J. Inherit. Metab. Dis. 30, 827.

Aoki, Y., Niihori, T., Kawame, H., Kurosawa, K., Ohashi, H., Tanaka, Y., Filocamo, M., Kato, K., Suzuki, Y., Kure, S., et al., 2005. Germline mutations in HRAS proto-oncogene cause Costello syndrome. Nat. Genet. 37, 1038–1040.

Aoki, Y., Niihori, T., Narumi, Y., Kure, S., Matsubara, Y., 2008. The RAS/MAPK syndromes: novel roles of the RAS pathway in human genetic disorders. Hum. Mutat. 29, 992–1006.

Aoki, Y., Niihori, T., Inoue, S., Matsubara, Y., 2016. Recent advances in RASopathies. J. Hum. Genet. 61, 33–39.

Avni, F.E., Guissard, G., Hall, M., Janssen, F., DeMaertelaer, V., Rypens, F., 2002. Hereditary polycystic kidney diseases in children: changing sonographic patterns through childhood. Pediatr. Radiol. 32, 169–174.

Biaglow, J.E., Cerniglia, G., Tuttle, S., Bakanauskas, V., Stevens, C., McKenna, G., 1997. Effect of oncogene transformation of rat embryo cells on cellular oxygen consumption and glycolysis. Biochem. Biophys. Res. Commun. 235, 739–742.

Bryant, K.L., Mancias, J.D., Kimmelman, A.C., Der, C.J., 2014. KRAS: feeding pancreatic cancer proliferation. Trends Biochem. Sci. 39, 91–100.

Carling, D., 2004. The AMP-activated protein kinase cascade—a unifying system for energy control. Trends Biochem. Sci. 29, 18–24.

Chen, X., Mitsutake, N., LaPerle, K., Akeno, N., Zanzonico, P., Longo, V.A., Mitsutake, S., Kimura, E.T., Geiger, H., Santos, E., et al., 2009. Endogenous expression of Hras(G12V) induces developmental defects and neoplasms with copy number imbalances of the oncogene. Proc. Natl. Acad. Sci. U. S. A. 106, 7979–7984.

Costello, J.M., 1977. A new syndrome: mental subnormality and nasal papillomata. Australian Paediatric J. 13, 114–118.

Folch, J., Lees, M., Sloane Stanley, G.H., 1957. A simple method for the isolation and purification of total lipides from animal tissues. J. Biol. Chem. 226, 497–509.

Fromenty, B., Pessayre, D., 1997. Impaired mitochondrial function in microvesicular steatosis. Effects of drugs, ethanol, hormones and cytokines. J. Hepatol. 26 (Suppl. 2), 43–53.

Fromenty, B., Berson, A., Pessayre, D., 1997. Microvesicular steatosis and steatohepatitis: role of mitochondrial dysfunction and lipid peroxidation. J. Hepatol. 26 (Suppl. 1), 13–22.
Fu, X., Iga, M., Kimura, M., Yamaguchi, S., 2000. Simplified screening for organic acidemia using GC/MS and dried urine filter paper: a study on neonatal mass screening. Early Hum. Dev. 58, 41–55.
Gilbert, E., Morel, A., Tulliez, M., Maunoury, R., Terzi, F., Miquerol, L., Kahn, A., 1997. In vivo effects of activated H-ras oncogene expressed in the liver and in urogenital tissues. Int. J. Cancer 73, 749–756.
Gripp, K.W., Lin, A.E., Stabley, D.L., Nicholson, L., Scott Jr., C.I., Doyle, D., Aoki, Y., Matsubara, Y., Zackai, E.H., Lapunzina, P., et al., 2006. HRAS mutation analysis in Costello syndrome: genotype and phenotype correlation. Am. J. Med. Genet. A 140, 1–7.
Hardie, D.G., 2004. The AMP-activated protein kinase pathway—new players upstream and downstream. J. Cell Sci. 117, 5479–5487.
Hennekam, R.C., 2003. Costello syndrome: an overview. Am. J. Med. Genet. C: Semin. Med. Genet. 117c, 42–48.
Hori, T., Fukao, T., Kobayashi, H., Teramoto, T., Takayanagi, M., Hasegawa, Y., Yasuno, T., Yamaguchi, S., Kondo, N., 2010. Carnitine palmitoyltransferase 2 deficiency: the time-course of blood and urinary acylcarnitine levels during initial L-carnitine supplementation. Tohoku J. Exp. Med. 221, 191–195.
Ibdah, J.A., Paul, H., Zhao, Y., Binford, S., Salleng, K., Cline, M., Matern, D., Bennett, M.J., Rinaldo, P., Strauss, A.W., 2001. Lack of mitochondrial trifunctional protein in mice causes neonatal hypoglycemia and sudden death. J. Clin. Invest. 107, 1403–1409.
Inoue, S., Moriya, M., Watanabe, Y., Miyagawa-Tomita, S., Niihori, T., Oba, D., Ono, M., Kure, S., Ogura, T., Matsubara, Y., et al., 2014. New BRAF knockin mice provide a pathogenetic mechanism of developmental defects and a therapeutic approach in cardio-facio-cutaneous syndrome. Hum. Mol. Genet. 23, 6553–6566.
Inoue, S.I., Takahara, S., Yoshikawa, T., Niihori, T., Yanai, K., Matsubara, Y., Aoki, Y., 2017. Activated Braf induces esophageal dilation and gastric epithelial hyperplasia in mice. Hum. Mol. Genet. 26, 4715–4727.
Joyce, S., Gordon, K., Brice, G., Ostergaard, P., 2016. The lymphatic phenotype in Noonan and Cardiofaciocutaneous syndrome. 24, 690–696.
Kerr, B., Delrue, M.A., Sigaudy, S., Perveen, R., Marche, M., Burgelin, I., Stef, M., Tang, B., Eden, O.B., O'Sullivan, J., et al., 2006. Genotype-phenotype correlation in Costello syndrome: HRAS mutation analysis in 43 cases. J. Med. Genet. 43, 401–405.
Kimura, M., Yamamoto, T., Yamaguchi, S., 1999. Automated metabolic profiling and interpretation of GC/MS data for organic acidemia screening: a personal computer-based system. Tohoku J. Exp. Med. 188, 317–334.
Kleefstra, T., Wortmann, S.B., Rodenburg, R.J., Bongers, E.M., Hadzsiev, K., Noordam, C., van den Heuvel, L.P., Nillesen, W.M., Hollody, K., Gillessen-Kaesbach, G., et al., 2011. Mitochondrial dysfunction and organic aciduria in five patients carrying mutations in the Ras-MAPK pathway. Eur. J. Hum. Genet. 19, 138–144.
Kobayashi, H., Hasegawa, Y., Endo, M., Purevsuren, J., Yamaguchi, S., 2007. ESI-MS/MS study of acylcarnitine profiles in urine from patients with organic acidemias and fatty acid oxidation disorders. J. Chromatogr. B Anal. Technol. Biomed. Life Sci. 855, 80–87.
Lawrence, M.S., Stojanov, P., Mermel, C.H., Robinson, J.T., Garraway, L.A., Golub, T.R., Meyerson, M., Gabriel, S.B., Lander, E.S., Getz, G., 2014. Discovery and saturation analysis of cancer genes across 21 tumour types. Nature 505, 495–501.
Lee, J., Choi, J., Scafidi, S., Wolfgang, M.J., 2016. Hepatic fatty acid oxidation restrains systemic catabolism during starvation. Cell Rep. 16, 201–212.
Leoni, C., Onesimo, R., Giorgio, V., Diamanti, A., Giorgio, D., Martini, L., Rossodivita, A., Tartaglia, M., Zampino, G., 2016. Understanding growth failure in Costello syndrome: increased resting energy expenditure. J. Pediatr. 170, 322–324.
Matsumura, H., Hasuwa, H., Inoue, N., Ikawa, M., Okabe, M., 2004. Lineage-specific cell disruption in living mice by Cre-mediated expression of diphtheria toxin A chain. Biochem. Biophys. Res. Commun. 321, 275–279.
McDaniel, A.S., Zhai, Y., Cho, K.R., Dhanasekaran, S.M., Montgomery, J.S., Palapattu, G., Siddiqui, J., Morgan, T., Alva, A., Weizer, A., et al., 2014. HRAS mutations are frequent in inverted urothelial neoplasms. Hum. Pathol. 45, 1957–1965.
Mistilis, S.P., Skyring, A.P., Stephen, D.D., 1965. Intestinal lymphangiectasia mechanism of enteric loss of plasma-protein and fat. Lancet (London, England) 1, 77–79.
Moriya, M., Inoue, S., Miyagawa-Tomita, S., Nakashima, Y., Oba, D., Niihori, T., Hashi, M., Ohnishi, H., Kure, S., Matsubara, Y., et al., 2015. Adult mice expressing a Braf Q241R mutation on an ICR/CD-1 background exhibit a cardio-facio-cutaneous syndrome phenotype. Hum. Mol. Genet. 24, 7349–7360.
Myers, A., Bernstein, J.A., Brennan, M.L., Curry, C., Esplin, E.D., Fisher, J., Homeyer, M., Manning, M.A., Muller, E.A., Niemi, A.K., et al., 2014. Perinatal features of the RASopathies: noonan syndrome, cardiofaciocutaneous syndrome and costello syndrome. Am. J. Med. Genet. A 164a, 2814–2821.
Oliva, J.L., Zarich, N., Martinez, N., Jorge, R., Castrillo, A., Azanedo, M., Garcia-Vargas, S., Gutierrez-Eisman, S., Juarranz, A., Bosca, L., et al., 2004. The P34G mutation reduces the transforming activity of K-Ras and N-Ras in NIH 3T3 cells but not of H-Ras. J. Biol. Chem. 279, 33480–33491.
Olpin, S.E., Clark, S., Andresen, B.S., Bischoff, C., Olsen, R.K., Gregersen, N., Chakrapani, A., Downing, M., Manning, N.J., Sharrard, M., et al., 2005. Biochemical, clinical and molecular findings in LCHAD and general mitochondrial trifunctional protein deficiency. J. Inherit. Metab. Dis. 28, 533–544.
Rauen, K.A., 2013. The RASopathies. Annu. Rev. Genomics Hum. Genet. 14, 355–369.
Rubio-Gozalbo, M.E., Bakker, J.A., Waterham, H.R., Wanders, R.J., 2004. Carnitine-acylcarnitine translocase deficiency, clinical, biochemical and genetic aspects. Mol. Asp. Med. 25, 521–532.
Schaffner, D.L., Barrios, R., Massey, C., Banez, E.I., Ou, C.N., Rajagopalan, S., Aguilar-Cordova, E., Lebovitz, R.M., Overbeek, P.A., Lieberman, M.W., 1993. Targeting of the rasT24 oncogene to the proximal convoluted tubules in transgenic mice results in hyperplasia and polycystic kidneys. Am. J. Pathol. 142, 1051–1060.
Schuhmacher, A.J., Guerra, C., Sauzeau, V., Canamero, M., Bustelo, X.R., Barbacid, M., 2008. A mouse model for Costello syndrome reveals an Ang II-mediated hypertensive condition. J. Clin. Invest. 118, 2169–2179.
Son, J., Lyssiotis, C.A., Ying, H., Wang, X., Hua, S., Ligorio, M., Perera, R.M., Ferrone, C.R., Mullarky, E., Shyh-Chang, N., et al., 2013. Glutamine supports pancreatic cancer growth through a KRAS-regulated metabolic pathway. Nature 496, 101–105.
Tajan, M., Batut, A., Cadoudal, T., Deleruyelle, S., Le Gonidec, S., Saint Laurent, C., Vomscheid, M., Wanecq, E., Treguer, K., De Rocca Serra-Nedelec, A., et al., 2014. LEOPARD syndrome-associated SHP2 mutation confers leanness and protection from diet-induced obesity. Proc. Natl. Acad. Sci. U. S. A. 111, E4494–4503.
Takahashi, M., Ohashi, H., 2013. Craniofacial and dental malformations in Costello syndrome: a detailed evaluation using multi-detector row computed tomography. Congenit. Anom. 53, 67–72.
Telang, S., Lane, A.N., Nelson, K.K., Arumugam, S., Chesney, J., 2007. The oncoprotein H-RasV12 increases mitochondrial metabolism. Mol. Cancer 6, 77.
Tian, W.N., Braunstein, L.D., Pang, J., Stuhlmeier, K.M., Xi, Q.C., Tian, X., Stanton, R.C., 1998. Importance of glucose-6-phosphate dehydrogenase activity for cell growth. J. Biol. Chem. 273, 10609–10617.
Tidyman, W.E., Rauen, K.A., 2009. The RASopathies: developmental syndromes of Ras/MAPK pathway dysregulation. Curr. Opin. Genet. Dev. 19, 230–236.
Trietsch, M.D., Spaans, V.M., ter Haar, N.T., Osse, E.M., Peters, A.A., Gaarenstroom, K.N., Fleuren, G.J., 2014. CDKN2A(p16) and HRAS are frequently mutated in vulvar squamous cell carcinoma. Gynecol. Oncol. 135, 149–155.
Unterberger, E.B., Eichner, J., Wrzodek, C., Lempiainen, H., Luisier, R., Terranova, R., Metzger, U., Plummer, S., Knorpp, T., Braeuning, A., et al., 2014. Ha-ras and beta-catenin oncoproteins orchestrate metabolic programs in mouse liver tumors. Int. J. Cancer 135, 1574–1585.
Urosevic, J., Sauzeau, V., Soto-Montenegro, M.L., Reig, S., Desco, M., Wright, E.M., Canamero, M., Mulero, F., Ortega, S., Bustelo, X.R., et al., 2011. Constitutive activation of B-Raf in the mouse germ line provides a model for human cardio-facio-cutaneous syndrome. Proc. Natl. Acad. Sci. U. S. A. 108, 5015–5020.
Vignes, S., Bellanger, J., 2008. Primary intestinal lymphangiectasia (Waldmann's disease). Orphanet J. of Rare Dis. 3, 5.
Viosca, J., Schuhmacher, A.J., Guerra, C., Barco, A., 2009. Germline expression of H-Ras(G12V) causes neurological deficits associated to Costello syndrome. Genes Brain Behav. 8, 60–71.
Vishwanath, V.A., 2016. Fatty acid Beta-oxidation disorders: a brief review. Ann. Neurosci. 23, 51–55.
Warburg, O., 1956. On the origin of cancer cells. Science (New York, N.Y.) 123, 309–314.
Wey, M., Lee, J., Jeong, S.S., Kim, J., Heo, J., 2013. Kinetic mechanisms of mutation-dependent Harvey Ras activation and their relevance for the development of Costello syndrome. Biochemistry 52, 8465–8479.
Wu, X., Simpson, J., Hong, J.H., Kim, K.H., Thavarajah, N.K., Backx, P.H., Neel, B.G., Araki, T., 2011. MEK-ERK pathway modulation ameliorates disease phenotypes in a mouse model of Noonan syndrome associated with the Raf1(L613V) mutation. J. Clin. Invest. 121, 1009–1025.
Yang, D., Wang, M.T., Tang, Y., Chen, Y., Jiang, H., Jones, T.T., Rao, K., Brewer, G.J., Singh, K.K., Nie, D., 2010. Impairment of mitochondrial respiration in mouse fibroblasts by oncogenic H-RAS(Q61L). Cancer Biol. & Ther. 9, 122–133.
Zheng, W., Tayyari, F., Gowda, G.A., Raftery, D., McLamore, E.S., Porterfield, D.M., Donkin, S.S., Bequette, B., Teegarden, D., 2015. Altered glucose metabolism in Harvey-ras transformed MCF10A cells. Mol. Carcinog. 54, 111–120.
Zhou, X., Zheng, W., Nagana Gowda, G.A., Raftery, D., Donkin, S.S., Bequette, B., Teegarden, D., 2016. 1,25-Dihydroxyvitamin D inhibits glutamine metabolism in Harvey-ras transformed MCF10A human breast epithelial cell. J. Steroid Biochem. Mol. Biol. 163, 147–156.